Eur J Nucl Med Mol Imaging (2012) 39:481–492
DOI 10.1007/s00259-011-1992-9

ORIGINAL ARTICLE

Comparative evaluation of synthetic anti-HER2 Affibody molecules site-specifically labelled with ^{111}In using N-terminal DOTA, NOTA and NODAGA chelators in mice bearing prostate cancer xenografts

Jennie Malmberg · Anna Perols · Zohreh Varasteh · Mohamed Altai · Alexis Braun · Mattias Sandström · Ulrike Garske · Vladimir Tolmachev · Anna Orlova · Amelie Eriksson Karlström

Received: 17 August 2011 / Accepted: 2 November 2011 / Published online: 30 November 2011

Abstract
Purpose In disseminated prostate cancer, expression of human epidermal growth factor receptor type 2 (HER2) is one of the pathways to androgen independence. Radionuclide molecular imaging of HER2 expression in disseminated prostate cancer might identify patients for HER2-targeted therapy. Affibody molecules are small (7 kDa) targeting proteins with high potential as tracers for radionuclide imaging. The goal of this study was to develop an optimal Affibody-based tracer for visualization of HER2 expression in prostate cancer.
Methods A synthetic variant of the anti-HER2 $Z_{HER2:342}$ Affibody molecule, $Z_{HER2:S1}$, was N-terminally conjugated with the chelators DOTA, NOTA and NODAGA. The conjugated proteins were biophysically characterized by electrospray ionization mass spectroscopy (ESI-MS), circular dichroism (CD) spectroscopy and surface plasmon resonance (SPR)-based biosensor analysis. After labelling with ^{111}In, the biodistribution was assessed in normal mice and the two most promising conjugates were further evaluated for tumour targeting in mice bearing DU-145 prostate cancer xenografts.
Results The HER2-binding equilibrium dissociation constants were 130, 140 and 90 pM for DOTA-$Z_{HER2:S1}$, NOTA-$Z_{HER2:S1}$ and NODAGA-$Z_{HER2:S1}$, respectively. A comparative study of ^{111}In-labelled DOTA-$Z_{HER2:S1}$, NOTA-$Z_{HER2:S1}$ and NODAGA-$Z_{HER2:S1}$ in normal mice demonstrated a substantial influence of the chelators on the biodistribution properties of the conjugates. ^{111}In-NODAGA-$Z_{HER2:S1}$ had the most rapid clearance from blood and healthy tissues. ^{111}In-NOTA-$Z_{HER2:S1}$ showed high hepatic uptake and was excluded from further evaluation. ^{111}In-DOTA-$Z_{HER2:S1}$ and ^{111}In-NODAGA-$Z_{HER2:S1}$ demonstrated specific uptake in DU-145 prostate cancer xenografts in nude mice. The tumour uptake of ^{111}In-NODAGA-$Z_{HER2:S1}$, 5.6±0.4%ID/g, was significantly lower than the uptake of ^{111}In-DOTA-$Z_{HER2:S1}$, 7.4±0.5%ID/g, presumably because of lower bioavailability due to more rapid clearance. ^{111}In-NODAGA-$Z_{HER2:S1}$ provided higher tumour-to-blood ratio, but somewhat lower tumour-to-liver, tumour-to-spleen and tumour-to-bone ratios.

Jennie Malmberg and Anna Perols contributed equally to this study.

J. Malmberg · Z. Varasteh · A. Orlova
Preclinical PET Platform, Department of Medicinal Chemistry,
Uppsala University,
Uppsala, Sweden

A. Perols · A. Braun · A. Eriksson Karlström (✉)
Division of Molecular Biotechnology, School of Biotechnology,
KTH Royal Institute of Technology, AlbaNova University Centre,
106 91 Stockholm, Sweden
e-mail: amelie@biotech.kth.se

M. Altai · V. Tolmachev
Unit of Biomedical Radiation Sciences, Rudbeck Laboratory,
Uppsala University,
Uppsala, Sweden

M. Sandström
Section of Medical Physics, Department of Oncology,
Uppsala University Hospital,
Uppsala, Sweden

U. Garske
Department of Medical Sciences, Section of Nuclear Medicine,
Uppsala University Hospital,
751 85 Uppsala, Sweden

Conclusion Since distant prostate cancer metastases are situated in bone or bone marrow, the higher tumour-to-bone ratio is the most important. This renders ^{111}In-DOTA-$Z_{HER2:S1}$ a preferable agent for imaging of HER2 expression in disseminated prostate cancer.

Keywords HER2 expression · Affibody molecule · Radionuclide molecular imaging · Prostate cancer · Macrocyclic chelators

Introduction

Treatment of disseminated prostate cancer (PC) is a challenge. The proliferation of PC cells is initially testosterone driven. The first line of treatment is a chemical or surgical castration, which can result in a clinically stable state lasting 1–2 years. During this time the androgen ablation therapy will suppress tumour growth, but promote a cellular selection favouring cells with a phenotype that allows for proliferation in the absence of androgen. Eventually this cellular selection will lead to an alteration in the phenotypic profile of the tumour making it less susceptible to the growth-suppressing influence of androgen ablation and indicating a preferable starting point for a second-line treatment.

Previous studies have confirmed a positive correlation between this progression toward androgen independence and an increase in the cellular expression of the human epidermal growth factor receptor type 2 (also referred to as HER2 or ErbB2) [1]. The receptor is a transmembrane tyrosine kinase (Trk) belonging to the HER (ErbB) family of TrK receptors and activates a pathway that promotes cell division and suppression of apoptosis, and increases cell motility [2]. Unlike other kinases, HER2 is able to activate the androgen receptor (AR) pathway, even in the absence of androgens [3–5]. This provides a selective survival and growth advantage for HER2-expressing subpopulations of cells and accelerates the progression of the tumour towards androgen independence. The process is associated with aggressive behaviour and renders the cells more resistant to therapy [6–8] in a similar manner that can be observed for other types of cancer displaying a high HER2 expression [9]. Although the HER2 expression level is rather weak, between 1+ and 2+ staining according to the HercepTest criteria, there is a strong correlation between this expression and high Gleason grade, advanced pT stage, rapid tumour cell proliferation and tumour recurrence [8], i.e. this level of expression has a strong prognostic value.

Radionuclide molecular imaging might be utilized to follow the progression of the disease by visualizing these changes in the phenotypic profile of the tumour. Accurate molecular phenotyping might suggest the most suitable molecular targets for a second-line therapy making the treatment of androgen-independent PC more personalized. A challenge is the heterogeneity of gene expression in metastases. The use of radionuclide molecular imaging would enable repeated imaging of aberrant expression of different gene products in all metastases simultaneously. Moreover, the use of contemporary combined imaging devices [positron emission tomography (PET)/CT or single photon emission computed tomography (SPECT)/CT] would provide anatomical landmarks for the biochemical changes.

Initially, anti-HER2 monoclonal antibodies were evaluated for imaging of HER2 expression in malignant tumours [10]. The data demonstrated satisfactory imaging contrast in xenografts with high HER2 expression (e.g. breast and ovarian carcinomas), although the long residence time of monoclonal antibodies in blood adversely influenced the contrast. Data from previous studies indicate that HER2 may be a valid imaging target in androgen-independent PC [11]. However, HER2 imaging in PC poses a crucial challenge as, unlike in breast or ovarian carcinomas, HER2 expression levels in PC are moderate [8] and hence the receptor detectability is lower. Therefore, selecting a targeting agent capable of producing high-contrast images when a target protein is moderately expressed is essential.

Affibody molecules are a new class of small (6.5 kDa) scaffold-based affinity proteins, which have shown a high potential as targeting probes for radionuclide imaging [12–14]. Derivatives of the anti-HER2 $Z_{HER2:342}$ Affibody molecule [15] have demonstrated excellent capacity for HER2 imaging in breast, colon and ovarian carcinoma xenografts [13]. A pilot clinical study confirmed that ^{111}In- and ^{68}Ga-labelled $Z_{HER2:342}$ can visualize HER2-expressing breast cancer metastases [16]. In addition, a comparative study confirmed the higher efficacy of $Z_{HER2:342}$ for visualization of PC xenografts in comparison with intact IgG [17].

Previous studies have demonstrated that the biodistribution of Affibody molecules can be appreciably influenced by the chemistry applied for labelling. It has been shown that minimal changes in the composition of peptide-based N_3S chelators for ^{99m}Tc can significantly alter the predominant excretion route [18–20], hepatic uptake [21] and renal retention of radioactivity [22, 23]. Different chelators for ^{111}In, when coupled to the C terminus, influence the clearance rate, which results in substantially different tumour-to-organ ratios [24]. These data suggested that it is possible to optimize imaging properties, i.e. tumour-to-organ ratios, which determine contrast and, in turn, sensitivity of imaging, of Affibody molecules by optimizing the labelling chemistry. This is especially important when up-regulation of a molecular target leads to moderate expression levels, as in the case of HER2 in PC.

The homologous macrocyclic chelators 1,4,7,10-tetraazacyclododecane-1,4,7,10-tetraacetic acid (DOTA),

1,4,7-triazacyclononane-*N*,*N*′,*N*″-triacetic acid (NOTA) and 1-(1,3-carboxypropyl)-4,7-carboxymethyl-1,4,7-triazacyclononane (NODAGA) are known to form stable complexes in vivo with the radionuclide ^{111}In, which is suitable for SPECT imaging [24–26]. At the same time, they differ in coordination chemistry and in net charge. We hypothesized that these subtle differences might be sufficient to modify the biodistribution of $Z_{HER2:342}$ and allow for selection of a variant with the highest sensitivity for imaging of HER2 expression in PC.

To verify this hypothesis, the DOTA, NOTA and NODAGA chelators were introduced at the N-terminus of a synthetic variant of the $Z_{HER2:342}$ Affibody molecule (Fig. 1). The conjugates were labelled with ^{111}In, and their biodistribution was compared in a murine model.

Materials and methods

General

Buffers, including 0.1 M phosphate-buffered saline (PBS), pH 7.5, and 0.2 M ammonium acetate, pH 5.5, were prepared using common methods from chemicals supplied by Merck (Darmstadt, Germany). High-quality Milli-Q© water (resistance higher than 18 MΩ cm) was used for preparing the solutions. Buffers, which were used for conjugation and labelling, were purified from metal contamination using Chelex 100 resin (Bio-Rad Laboratories, Richmond, CA, USA). [^{111}In]indium chloride was purchased from Covidien (Hazelwood, MO, USA). Radioactivity was measured with an automated gamma counter with 3-in. NaI(Tl) detector (1480 WIZARD, Wallac Oy, Turku, Finland). The data were corrected for dead time and background.

Synthesis and characterization of DOTA-, NOTA- and NODAGA-conjugated Affibody molecules

A synthetic variant of the $Z_{HER2:342}$ Affibody molecule, here denoted $Z_{HER2:S1}$, with the sequence AEAKYA KEMRNAYWEIALLPNLNNQQKRAFIRSLYDDPSQ SANLLAEAKKLNDAQAPK-amide was assembled on a 433A Peptide Synthesizer (Applied Biosystems, Foster City, CA, USA) using Fmoc/tBu chemistry in 0.1 mmol scale with underlined residues coupled twice. Fmoc-protected amino acids with standard side chain protecting groups were obtained from Novabiochem (Merck, Darmstadt, Germany), Iris Biotech (Marktredwitz, Germany) and Applied Biosystems. For preparation of the NODAGA conjugate (PEP10417) and DOTA conjugate (PEP10415), Fmoc-Rink amide resin (Novabiochem) was used for assembly of the Affibody molecule essentially as described in [27]. As the final step of the synthesis the *tert*-butyl-protected monoreactive chelators DOTA (Macrocyclics, Dallas, TX, USA) and NODAGA (CheMatech, Dijon, France) were manually conjugated to the N-terminal of the protein using 5 eq of chelator, 5 eq of 2-(7-aza-1H-benzotriazole-1-yl)-1,1,3,3-tetramethyluronium hexafluorophosphate (HATU) (Atlantic SciTech Group, Inc., Linden, NJ, USA) and 5 eq of diisopropylethylamine (DIEA) (Applied Biosystems) in *N*-methylpyrrolidone (NMP) at room temperature (RT) overnight. Ninhydrin tests were used to monitor the reaction, and additional conjugations were performed if the test gave a positive result. For preparation of the NOTA conjugate (PEP10416), the Affibody molecule was assembled on amino-PEGA-resin (Novabiochem) functionalized with Fmoc-Rink amide linker (Novabiochem), using the synthetic protocol described above. Unprotected NOTA (CheMatech, Dijon, France) was conjugated to the N-terminal using 5 eq of 1-ethyl-3-(3-dimethylaminopropyl)carbodiimide (EDC) (Advanced ChemTech, Louisville, KY, USA), 5 eq of *N*-hydroxysuccinimide (NHS) (Bachem, Bubendorf, Switzerland) and 5 eq of DIEA in 50% dimethylformamide (DMF)-water at RT for 2 h. Removal of side chain-protecting groups and cleavage of the protein from the resin were performed in a single-step treatment for 3 h with TFA (Apollo Scientific):TIS (Aldrich):H_2O (95:2.5:2.5) for all variants. Proteins were extracted in *tert*-butyl methyl ether (Merck):water (50:50) three times before the water phase was filtered and lyophilized.

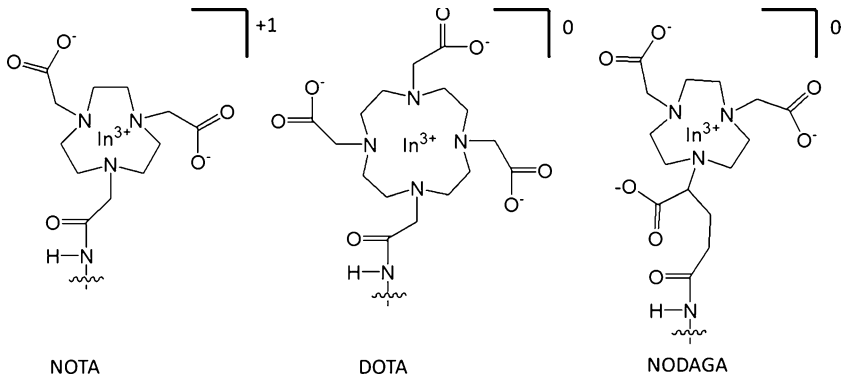

Fig. 1 Schematic overview illustrating the structural differences of the three chelators, 1,4,7-triazacyclononane-*N*,*N*′,*N*″-triacetic acid (NOTA), 1,4,7,10-tetraazacyclododecane-1,4,7,10-tetraacetic acid (DOTA) and 1-(1,3-carboxypropyl)-4,7-carboxymethyl-1,4,7-triazacyclononane (NODAGA), including the net charges of the In^{3+} complexes

The crude synthetic product was analysed using RP-HPLC (1200 series, Agilent). For purification, a semi-preparative column, Reprosil Gold 10×250 mm, 5 μm particle size (Dr. Maisch, Ammerbuch, Germany) was used with a flow rate of 3.5 ml/min and a gradient of 25–45% B (A: 0.1% TFA:H_2O and B: 0.1% TFA:CH_3CN) over 25 min. Purity analysis was performed with an analytical column, Zorbax CB300-C18 4.6×150 mm, 3.5 μm particle size (Agilent) and a flow rate of 1 ml/min. Verification of the correct products was performed by electrospray ionization quadrupole time-of-flight mass spectrometry (ESI-Q-TOF-MS) (Agilent). The concentrations of the purified proteins were determined by amino acid analysis (Aminosyraanalyscentralen, Uppsala, Sweden).

Variable temperature measurements in order to determine the melting point for the conjugates were performed using a JASCO-810 spectropolarimeter (Jasco, Tokyo, Japan) as described earlier [24]. In order to make sure that the Affibody molecules retained their affinity after chelator conjugation, real-time biosensor analysis on a Biacore 3000 (GE Healthcare) was used. The kinetic constants for the interaction between the conjugates and the extracellular domain of HER2 were determined by surface plasmon resonance using a Biacore 3000 system as described earlier [24]. In short, recombinantly produced extracellular domain of human HER2 expressed as an Fc-fusion protein (R&D Systems, Minneapolis, MN, USA) was immobilized on a carboxylated dextran-coated CM5 sensor chip using EDC/NHS chemistry. The three conjugates were diluted in 1× HBS-ET running buffer [10 mM hydroxyethyl piperazine ethanesulfonic acid (HEPES), 150 mM NaCl, 3.4 mM ethylenediaminetetraacetic acid (EDTA), 0.05% Tween 20, pH 7.4] to six concentrations ranging from 0.3 to 10 nM. Duplicates of concentrations were analysed with an association phase of 5 min followed by 10 min dissociation before the surface was regenerated with a short pulse of 25 mM HCl. Kinetic analysis was performed using BiaEval 4.1 software with a 1:1 Langmuir binding model.

Labelling chemistry

For labelling with ^{111}In, $Z_{HER2:S1}$-based conjugates were reconstituted in 0.2 M ammonium acetate buffer, pH 5.5, to a concentration of 1 mg/ml. For typical labelling, 30 μl of the $Z_{HER2:S1}$ solution was mixed with 50 μl 0.2 M ammonium acetate buffer, pH 5.5, and 30–70 MBq of ^{111}In-indium chloride (80–160 μl solution in 0.05 M HCl). With NOTA and DOTA the reaction mixture was incubated at 60°C for 30 min and with NODAGA incubation took place at 90°C for 30 min, and radiochemical purity was evaluated. The measurement of radiochemical yield and purity was performed by instant thin-layer chromatography (ITLC) using Tec-Control Chromatography 150–771 (Biodex Medical Systems, Shirley, NY, USA), and distribution of radioactivity along the ITLC strips was measured on a Cyclone™ Storage Phosphor System and analysed using the OptiQuant™ image analysis software. The accuracy of radio-ITLC analysis was cross-validated by sodium dodecyl sulfate polyacrylamide gel electrophoresis (SDS-PAGE).

Due to high yield, no additional purification of ^{111}In-DOTA-$Z_{HER2:S1}$ and ^{111}In-NOTA-$Z_{HER2:S1}$ was required. ^{111}In-NODAGA-$Z_{HER2:S1}$ was purified using disposable size-exclusion columns NAP-5 (GE Healthcare, Uppsala, Sweden) pre-equilibrated and eluted with PBS.

To evaluate the stability of labelling, the ^{111}In-labelled conjugates were incubated with 1,000-fold excess of EDTA for 4 h and then analysed using ITLC.

In vitro studies

PC cell lines DU-145 (51,000±14,000 receptors per cell [11]) and PC3 (23,600±8,500 receptors per cell [11]) were used for in vitro binding specificity tests. According to Ross and coworkers [28], such expression levels correspond to 1+ staining using standard immunohistochemistry protocols. In addition, the ovarian cancer cell line SKOV-3 with high HER2 expression (1,200,000 ±100,000 receptors per cell [29]) was utilized for the evaluation of cellular binding and processing. All cell lines were purchased from the American Type Culture Collection (ATCC). Cells were cultivated in a humidified incubator with 5% CO_2 at 37°C in complete RPMI media, supplemented with 10% fetal bovine serum (FBS), 2 mM L-glutamine, 100 IU/ml penicillin and 100 μg/ml of streptomycin. All reagents including media and trypsin-EDTA were from Biochrom KG, Berlin, Germany.

An in vitro specificity test was performed according to the method described earlier [30]. Briefly, a solution of tested radiolabelled conjugate (0.008 ng, 1 nM) was added to six petri dishes (ca. 10^6 cells in each). For blocking, a 500-fold excess of non-labelled recombinant $Z_{HER2:342}$ was added 10 min before the labelled conjugate to saturate the receptors. The cells were incubated for 1 h in a humidified incubator at 37°C. Thereafter, the media were collected, the cells were detached by trypsin-EDTA solution and the radioactivity in cells and media was measured to calculate a percentage of cell-bound radioactivity.

Internalization of ^{111}In-DOTA-$Z_{HER2:S1}$, ^{111}In-NOTA-$Z_{HER2:S1}$ and ^{111}In-NODAGA-$Z_{HER2:S1}$ was evaluated as described by Wållberg and Orlova [30]. SKOV-3 cells were incubated with 1 nM of ^{111}In-DOTA-$Z_{HER2:S1}$, ^{111}In-NOTA-$Z_{HER2:S1}$ or ^{111}In-NODAGA-$Z_{HER2:S1}$ in complete medium at 37°C. After 60 min incubation, the media with labelled compound were removed and the cells were washed three times with ice-cold serum-free medium. Complete medium (1 ml) was added to each cell dish and

the cells were further incubated at 37°C, 5% CO_2. At designated times during the incubation (0.5, 1, 2, 3, 4, 8 and 24 h), one group of three dishes was analysed for cell-associated radioactivity. The incubation medium was collected. Membrane-bound radioactivity was determined by treatment with 0.5 ml 4 M urea solution in a 0.1 M glycine buffer, pH 2.5, for 5 min on ice. The acid fraction was collected, and the cells were washed with an additional 0.5 ml acid solution, which was added to the acid fraction. Subsequently, the cells were lysed and collected for the measurement of internalized radioactivity. For lysis, 0.5 ml of 1 M sodium hydroxide solution was added, and the cells were incubated at 37°C for at least 0.5 h. The basic solution was collected. Dishes were washed with an additional 0.5 ml basic solution, and the basic fractions were pooled.

The radioactivity content of the samples was measured using an automated gamma counter, and data were normalized to the maximum uptake. Radioactivity measured in the acidic fraction represented membrane-bound radioactivity and in the alkaline fraction, it represented the internalized one.

Animal studies

All animal experiments were planned and performed in accordance with national legislation on laboratory animals' protection. The studies had been approved by the Local Ethics Committee for Animal Research.

In a typical experiment, a group of four mice was intravenously injected (tail vein) with 1 μg (30 kBq) of ^{111}In-DOTA-$Z_{HER2:S1}$, ^{111}In-NOTA-$Z_{HER2:S1}$ or ^{111}In-NODAGA-$Z_{HER2:S1}$ in 100 μl PBS each. Animals were euthanized by an intraperitoneal injection with a lethal dose of anaesthesia (10:1 Ketalar-Rompun solution, 20 μl per g of body weight) and subsequently subjected to heart puncture with a heparin-rinsed syringe. Samples or whole organs were collected from blood, lung, liver, spleen, colon, kidney, tumour (when xenografted), muscle and bone. Immediately following dissections, organs and tissue samples were weighed and their radioactivity was measured by automatic gamma spectrometer. The background was measured for each sample holder in the same way. Counting time was selected to provide at least 1,000 counts for samples with the lowest radioactivity. The organ uptake values were expressed as percent of injected dose per gram of tissue (%ID/g), except for the intestines and the remaining carcass where values were expressed as %ID per whole sample. All measurements were properly corrected for decay.

Biodistribution of ^{111}In-DOTA-$Z_{HER2:S1}$, ^{111}In-NOTA-$Z_{HER2:S1}$ or ^{111}In-NODAGA-$Z_{HER2:S1}$ was compared in male non-tumour-bearing NMRI mice (Taconic, Denmark) at 1, 4 and 24 h. The average animal weight was 26.8±1.7 g at the time of the experiment. The radiochemical purity of injected conjugates was 98.9, 98.2 and 99.4% for ^{111}In-DOTA-$Z_{HER2:S1}$, ^{111}In-NOTA-$Z_{HER2:S1}$ and ^{111}In-NODAGA-$Z_{HER2:S1}$, respectively.

Experiments in tumour-bearing mice were performed with ^{111}In-DOTA-$Z_{HER2:S1}$ and ^{111}In-NODAGA-$Z_{HER2:S1}$, which had demonstrated the most favourable biodistribution in normal mice. The DU-145 PC cell line (originating from PC brain metastasis) was used for xenografts. This cell line expresses $(5.1\pm1.4)\times10^4$ HER2 receptors per cell [11]. Male NMRI *nu/nu* mice (Taconic, Denmark) were subcutaneously grafted with 5×10^6 DU-145 cells (cell suspension in 100 μl Matrigel/HEPES salt solution, 1:1) on their right hind leg. The experiments were performed 3 weeks after implantation. The average tumour weight was 0.9±0.5 g at the time of the experiment. The average animal weight was 30.2±1.8 g at the time of the experiment.

For the in vivo specificity study in tumour-bearing mice, 16 mice with DU-145 xenografts were randomly divided into 4 equal groups. Two groups of mice were intravenously injected with 1 μg (30 kBq) of ^{111}In-DOTA-$Z_{HER2:S1}$ 100 μl PBS each, and another two groups with the same amount of ^{111}In-NODAGA-$Z_{HER2:S1}$. The radiochemical purity of injected conjugates was 98.2 and 99.5% for ^{111}In-DOTA-$Z_{HER2:S1}$ and ^{111}In-NODAGA-$Z_{HER2:S1}$, respectively. To confirm that the accumulation of conjugates in xenografts was HER2 specific, receptors in one group for each conjugate were pre-saturated by subcutaneous injection of 500 μg of unlabelled recombinant $Z_{HER2:342}$ 60 min prior to injection of the radiolabelled Affibody molecule, while another group was injected with the conjugate without pre-blocking. All animals were sacrificed at 4 h after injection, and the biodistribution of conjugates was measured as described above.

Biodistribution data were analysed by unpaired, two-tailed *t*-test using GraphPad Prism (version 4.00 for Windows GraphPad Software, San Diego, CA, USA) in order to determine any significant differences ($p<0.05$).

The distribution of ^{111}In-DOTA-$Z_{HER2:S1}$ and ^{111}In-NODAGA-$Z_{HER2:S1}$ in tumour-bearing mice was visualized by gamma-camera imaging. The conjugates (1 MBq, 1 μg) were administered by tail vein injection in NMRI *nu/nu* mice bearing established subcutaneous DU-145 tumour xenografts on right hind legs (two animals per conjugate). Then 4 h post injection, the mice were euthanized by an i.p. injection with a lethal dose (20 μl per g of body weight) of 10:1 Ketalar-Rompun solution and their bladders were removed. Imaging was performed with an Infinia VG (International General Electric, General Electric Medical Systems, Haifa, Israel). The dual-head gamma-camera was equipped with 3/8" thick NaI(Tl) crystals with a VPC-5 medium-energy general purpose collimator. An energy

Table 1 Biophysical characteristics of the Affibody conjugates

Conjugate	Purity	T_m	MW (Da)		Kinetic parameters				
					k_a ($M^{-1}\cdot s^{-1}$)		k_d (s^{-1})		K_D (M)
			Theor.	Exper.	Value	SE	Value	SE	
DOTA-$Z_{HER2:S1}$	98%	64°C	7,007	7,007	4.08×10^{6}	7.95×10^{3}	6.41×10^{-4}	2.18×10^{-6}	1.3×10^{-10}
NOTA-$Z_{HER2:S1}$	97%	63°C	6,907	6,907	5.68×10^{6}	2.19×10^{4}	7.98×10^{-4}	4.95×10^{-6}	1.4×10^{-10}
NODAGA-$Z_{HER2:S1}$	99%	63°C	6,977	6,977	6.57×10^{6}	1.32×10^{4}	5.89×10^{-4}	2.45×10^{-6}	9.0×10^{-11}

window of 20% was applied around the two dominant gamma ray energies of ^{111}In, 171 and 245 keV. A 60-min image with 256×256 matrix and a zoom factor of 2.0 was acquired. Evaluation of the images was performed with Osiris 4.0 software (Digital Imaging Unit, University Hospitals of Geneva, Switzerland).

Results

Synthesis and characterization of DOTA-, NOTA- and NODAGA-conjugated Affibody molecules

Peptide synthesis provided DOTA-$Z_{HER2:S1}$, NOTA-$Z_{HER2:S1}$ and NODAGA-$Z_{HER2:S1}$ with a purity of more than 95% (see Table 1). According to surface plasmon resonance measurements, the equilibrium dissociation constants (K_D) were 130, 140 and 90 pM for DOTA-$Z_{HER2:S1}$, NOTA-$Z_{HER2:S1}$ and NODAGA-$Z_{HER2:S1}$, respectively. The melting point of all conjugates was 63–64°C.

Labelling chemistry

The labelling yield of Affibody $Z_{HER2:S1}$ was 97±1% and 98±1% for ^{111}In-NOTA-$Z_{HER2:S1}$ and ^{111}In-DOTA-$Z_{HER2:S1}$, respectively, and no additional purification was required. For ^{111}In-NODAGA-$Z_{HER2:S1}$ the labelling yield was 51±5%. The purification of ^{111}In-NODAGA-$Z_{HER2:S1}$ with size exclusion chromatography provided a radiochemical purity of 99.5±0.2%. A challenge with 1,000-fold excess EDTA during 4 h demonstrated no measurable release of radioactivity from conjugates, which demonstrated a high stability of all labels.

In vitro studies

Binding specificity tests (Fig. 2) demonstrated that the binding of all ^{111}In-labelled conjugates to living HER2-expressing PC cell lines, as well as SKOV-3 cells, was receptor mediated, because saturation of the receptors by pre-incubation with non-labelled $Z_{HER2:S1}$ significantly decreased the binding of the radiolabelled Affibody molecule (for all studied cell lines, $p<0.0001$). The levels of cell-associated radioactivity were appreciably lower for non-blocked PC cells than for SKOV-3 cells, reflecting lower expression level of HER2.

Data concerning retention and cellular processing of ^{111}In-NOTA-$Z_{HER2:S1}$, ^{111}In-DOTA-$Z_{HER2:S1}$ and ^{111}In-NODAGA-$Z_{HER2:S1}$ are presented in Fig. 3. All conjugates demonstrated a similar processing pattern, which is typical for $Z_{HER2:342}$ and its derivatives. The overall retention of radioactivity was good, with 65–85% of activity still being cell associated after 24 h. The internalization rate of all three conjugates was slow, but internalized radioactivity was increasing throughout the duration of the study. There were, however, some chelator-related differences in internalized radioactivity. In the case of ^{111}In-DOTA-$Z_{HER2:S1}$, 31.7±0.6% of radioactivity was internalized at 24 h, while the corresponding value for ^{111}In-NOTA-$Z_{HER2:S1}$ was only 23±3%.

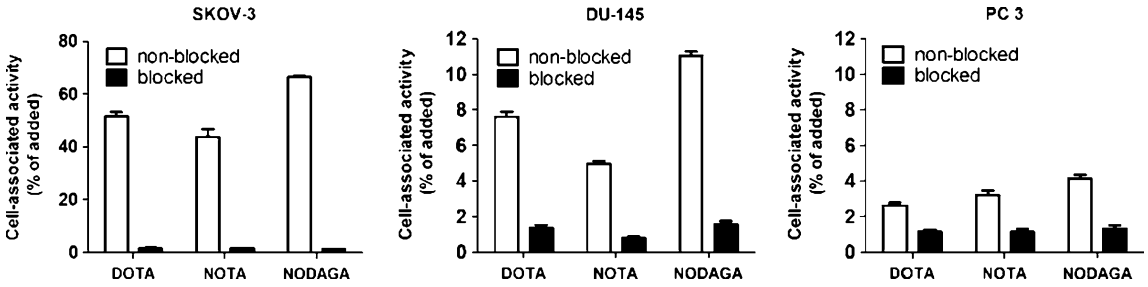

Fig. 2 Specificity of binding of ^{111}In-DOTA-$Z_{HER2:S1}$, ^{111}In-NOTA-$Z_{HER2:S1}$ and ^{111}In-NODAGA-$Z_{HER2:S1}$ to HER2-expressing cells in vitro. The test was performed on the ovarian cancer cell line, SKOV-3 (high expression level), and PC cell lines, DU-145 and PC-3 (both with low expression level). For pre-saturation of antigens, a 500-fold molar excess of non-radioactive Affibody molecules was added. Data are presented as mean values of percent added radioactivity that is cell bound from three cell dishes and standard deviations

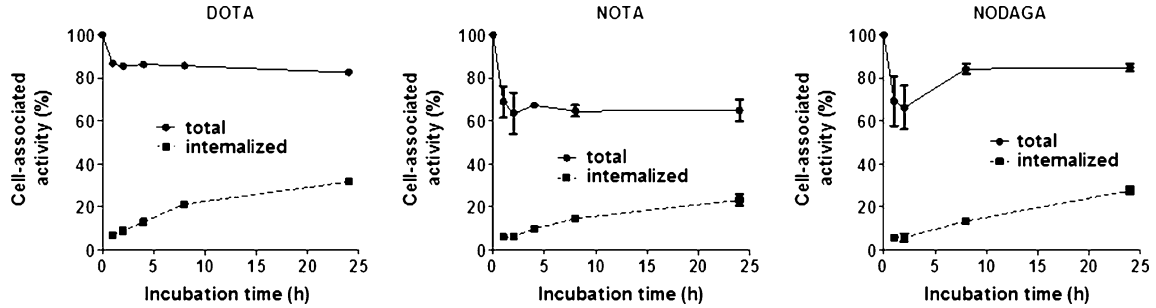

Fig. 3 In vitro cellular processing of ^{111}In-DOTA-$Z_{HER2:S1}$, ^{111}In-NOTA-$Z_{HER2:S1}$ and ^{111}In-NODAGA-$Z_{HER2:S1}$ bound to SKOV-3 cells. Cells were pre-incubated with the conjugates on ice, then the culture medium was changed and further incubation was performed at 37°C. Acid wash was used to discriminate between internalized and membrane-bound radioactivity. Data are presented as an average of three samples with standard deviations; error bars might not be seen because they are smaller than the symbols

Table 2 Comparative biodistribution of ^{111}In-NOTA-$Z_{HER2:S1}$, ^{111}In-DOTA-$Z_{HER2:S1}$ and ^{111}In-NODAGA-$Z_{HER2:S1}$ in male NMRI mice after intravenous injection

	^{111}In-NOTA-$Z_{HER2:S1}$	^{111}In-DOTA-$Z_{HER2:S1}$	^{111}In-NODAGA-$Z_{HER2:S1}$
	1 h after injection		
Blood	1.2±0.2[a]	1.8±0.1[b]	0.8±0.1[b]
Lung	1.6±0.2[a]	1.1±0.1	1.1±0.6
Liver	8.0±0.6[a]	2.9±0.1	2.5±0.4[b]
Spleen	3.2±1.3[a]	1.2±0.2[b]	0.71±0.05[b]
Colon	1.6±0.4[a]	0.6±0.1[b]	0.85±0.02[b]
Kidney	217±33[a]	170±17[b]	206±22
Muscle	0.3±0.2	0.41±0.09	0.3±0.1
Bone	2.2±1.8[a]	1.0±0.1[b]	1.4±0.1
GI tract with content	1.6±0.2	1.5±0.1	2.9±1.4
Carcass	13.1±0.8[a]	10.9±0.4	11.2±0.6[b]
	4 h after injection		
Blood	0.53±0.06	0.64±0.07[c]	0.08±0.02[b]
Lung	0.6±0.1[a]	0.50±0.07	0.42±0.05[b]
Liver	6.8±0.6[a]	2.9±0.3	2.7±0.2[b]
Spleen	1.0±0.3	0.8±0.2	0.6±0.2[b]
Colon	0.46±0.08[a]	0.29±0.06[c]	0.39±0.03
Kidney	184±28	162±22[c]	229±26
Muscle	0.19±0.03	0.22±0.02[c]	0.11±0.01[b]
Bone	1.0±0.1[a]	0.6±0.2[c]	0.89±0.05
GI tract with content	1.8±0.5[a]	0.9±0.2	1.1±0.2[b]
Carcass	6.4±0.4	7.0±0.9[c]	4.2±0.5[b]
	24 h after injection		
Blood	0.14±0.01	0.14±0.07[c]	0.01±0.00[b]
Lung	0.41±0.06[a]	0.2±0.1	0.17±0.03[b]
Liver	6.0±0.8[a]	2.43±0.02[c]	1.4±0.2[b]
Spleen	1.2±0.3[a]	0.7±0.2	0.4±0.1[b]
Colon	0.51±0.08[a]	0.30±0.06	0.20±0.02[b]
Kidney	148±2[a]	116±12	105±10[b]
Muscle	0.17±0.01	0.15±0.03[c]	0.05±0.01[b]
Bone	1.1±0.2[a]	0.5±0.2	0.48±0.04[b]
GI tract with content	1.3±0.3	1.0±0.3	0.61±0.30[b]
Carcass	5.5±0.7	5.7±0.3[c]	2.0±0.2[b]

Uptake is expressed as %ID/g and presented as an average value from four animals ± standard deviation (data for GI tract with content and carcass are presented as % of injected dose per whole sample)

[a]Significant difference (p <0.05) between ^{111}In-NOTA-$Z_{HER2:S1}$ and ^{111}In-DOTA-$Z_{HER2:S1}$

[b]Significant difference (p <0.05) between ^{111}In-NOTA-$Z_{HER2:S1}$ and ^{111}In-NODAGA-$Z_{HER2:S1}$

[c]Significant difference (p <0.05) between ^{111}In-DOTA-$Z_{HER2:S1}$ and ^{111}In-NODAGA-$Z_{HER2:S1}$

Animal studies

Data on the biodistribution of the radiolabelled conjugates in normal mice are presented in Table 2. All conjugates demonstrated rapid blood clearance and an overall low uptake in non-excretory organs. The low radioactivity level in the gastrointestinal (GI) tract indicated that the hepatobiliary pathway played a minor role in the excretion of all conjugates. On the opposite, the kidney radioactivity was high for all conjugates, which suggests predominantly renal excretion with subsequent re-absorption of conjugates in the proximal tubuli. Within this pattern, there was a clear chelator-dependent difference in the biodistribution of the conjugates. For example, the blood clearance of ^{111}In-NODAGA-$Z_{HER2:S1}$ was significantly more rapid, providing the lowest blood concentration throughout the study. This conjugate also provided the lowest lung uptake of the radioactivity. ^{111}In-NOTA-$Z_{HER2:S1}$ showed the highest liver uptake already 1 h after injection (8.0±0.6%ID/g), and the hepatic uptake of this conjugate remained more than twofold higher than the uptake of ^{111}In-DOTA-$Z_{HER2:S1}$ and ^{111}In-NODAGA-$Z_{HER2:S1}$ at 4 and 24 h after injection. As high liver uptake might prevent detection of hepatic metastases, this conjugate was excluded from further evaluation in tumour-bearing mice.

The data concerning biodistribution of ^{111}In-DOTA-$Z_{HER2:S1}$ and ^{111}In-NODAGA-$Z_{HER2:S1}$ in male NMRI *nu*/*nu* mice bearing DU-145 PC xenografts are presented in Table 3. Both conjugates have demonstrated highly specific tumour uptake. Pre-saturation of HER2 in tumours by pre-injection of non-labelled $Z_{HER2:342}$ caused significant ($p<0.0005$) reduction of radioactivity accumulation in xenografts for both conjugates. Pre-blocking did not cause significant differences in radioactivity concentration in normal organs and tissues. ^{111}In-NODAGA-$Z_{HER2:S1}$ cleared more rapidly from blood than ^{111}In-DOTA-$Z_{HER2:S1}$. The tumour uptakes (in non-blocked xenografts) were 7.4±0.4 and 5.6±0.4%ID/g for ^{111}In-DOTA-$Z_{HER2:S1}$ and ^{111}In-NODAGA-$Z_{HER2:S1}$, respectively. The data concerning tumour-to-organ ratio are presented in Fig. 4. The use of ^{111}In-NODAGA-$Z_{HER2:S1}$ provided significantly higher tumour-to-blood ratio (53±10 vs 26±3) in comparison with ^{111}In-DOTA-$Z_{HER2:S1}$. On the opposite, tumour-to-liver (5.6±0.5 vs 3.3±0.5), tumour-to-spleen (20±5 vs 10±3) and tumour-to-bone (29±8 vs 12±2) ratios were significantly higher for ^{111}In-DOTA-$Z_{HER2:S1}$.

Images acquired 4 h after the i.v. injection of the ^{111}In-DOTA-$Z_{HER2:S1}$ and ^{111}In-NODAGA-$Z_{HER2:S1}$ into mice bearing DU-145 xenografts confirmed the capacity of both conjugates to visualize HER2 expression (Fig. 5). In agreement with the biodistribution data, a prominent radioactivity uptake was observed in kidneys. No radioactivity accumulation in other healthy organs and tissues was observed.

Discussion

At progression, PC is often disseminated, androgen independent and non-responsive to treatment. Selective

Table 3 Comparative biodistribution of ^{111}In-DOTA-$Z_{HER2:S1}$ and ^{111}In-NODAGA-$Z_{HER2:S1}$ in male NMRI *nu*/*nu* mice bearing DU-145 PC xenografts 4 h after intravenous injection

	^{111}In-DOTA-$Z_{HER2:S1}$		^{111}In-NODAGA-$Z_{HER2:S1}$	
	Non-blocked	Blocked	Non-blocked	Blocked
Blood	0.28±0.04[b]	0.30±0.05	0.11±0.03	0.09±0.02
Lung	0.36±0.07	0.41±0.05	0.35±0.06	0.32±0.05
Liver	1.3±0.2	1.4±0.2	1.7±0.3	1.3±0.2
Spleen	0.4±0.1	0.5±0.1	0.6±0.2	0.39±0.08
Colon	0.32±0.09	0.26±0.04	0.35±0.05	0.38±0.06
Kidney	160±11	148±18	143±15	162±13
Muscle	0.09±0.01	0.09±0.01	0.08±0.01	0.08±0.01
Bone	0.3±0.1[b]	0.32±0.09	0.55±0.07	0.44±0.06
Tumour	7.4±0.4[a, b]	0.5±0.1	5.6±0.4[a]	0.6±0.1
GI tract with content	1.5±0.7	0.7±0.2	0.74±0.09	1.7±1.1
Carcass	4.3±0.8	4.7±0.5	4.2±0.6	4.3±0.3

Data are presented as an average %ID/g value from four animals ± standard deviation (data for intestines with content and carcass are presented as % of injected radioactivity per whole sample)

[a] Significant difference (p <0.05) between blocked and non-blocked groups

[b] Significant difference (p <0.05) between ^{111}In-DOTA-$Z_{HER2:S1}$ and ^{111}In-NODAGA-$Z_{HER2:S1}$ in non-blocked group

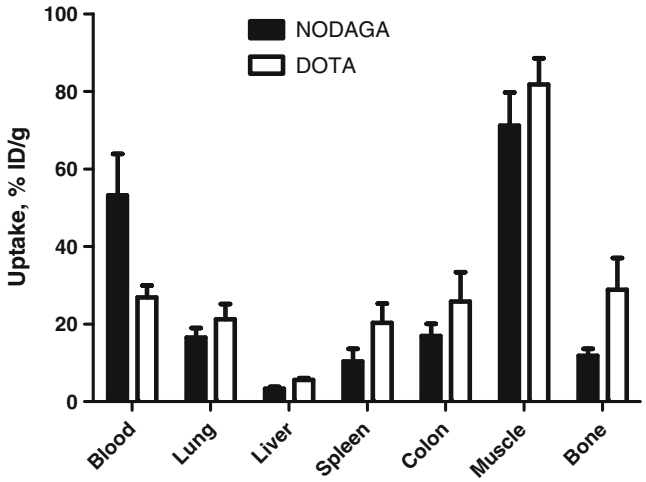

Fig. 4 Comparison of tumour-to-organ ratios for ^{111}In-DOTA-$Z_{HER2:S1}$ and ^{111}In-NODAGA-$Z_{HER2:S1}$ in NMRI *nu*/*nu* mice bearing DU-145 xenografts 4 h after injection. Differences in tumour-to-blood, tumour-to-liver, tumour-to-spleen and tumour-to-bone ratios were significant ($p<0.05$)

targeting of pathways that enable PC to proliferate without androgen stimulation is a promising approach to treatment of disseminated PC. One such promising molecular target is HER2 that is capable of inducing PC cell proliferation in the absence of androgen hormones by an outlaw pathway [31]. Several HER2-targeting drugs are approved or passing late stage clinical trials [32]. Although HER2-targeted therapy is so far mainly concentrated on breast cancer, its successful translation into treatment of other carcinomas, e.g. gastric cancer, has been demonstrated [33]. Nevertheless, clinical trials on treatment of PC with trastuzumab or lapatinib have failed to demonstrate efficacy as unselected patients were enrolled in these trials, and, at the best, only biopsies from primary tumours were analysed [34–36]. Patient stratification according to HER2 expression level was suggested as one possible way to improve therapy [34]. Radionuclide molecular imaging may become a powerful tool for identification of metastasis with an increased HER2 expression. Affibody molecules are well suited for such purposes and generate rapid high contrast for visualization of the phenotypic profile. A derivative of the $Z_{HER2:342}$ Affibody molecule has previously been demonstrated to be superior to radiolabelled trastuzumab for imaging of HER2-expressing PC xenografts [17]. One has to take into account that the HER2 expression level in PC is relatively moderate [8], in fact appreciably lower than in e.g. breast cancer. This motivates further optimization of the $Z_{HER2:342}$ Affibody molecule to develop conjugates providing the highest possible sensitivity. In this study, we evaluated a series of Affibody molecules with different chelators (DOTA, NOTA and NODAGA) at the N-terminus.

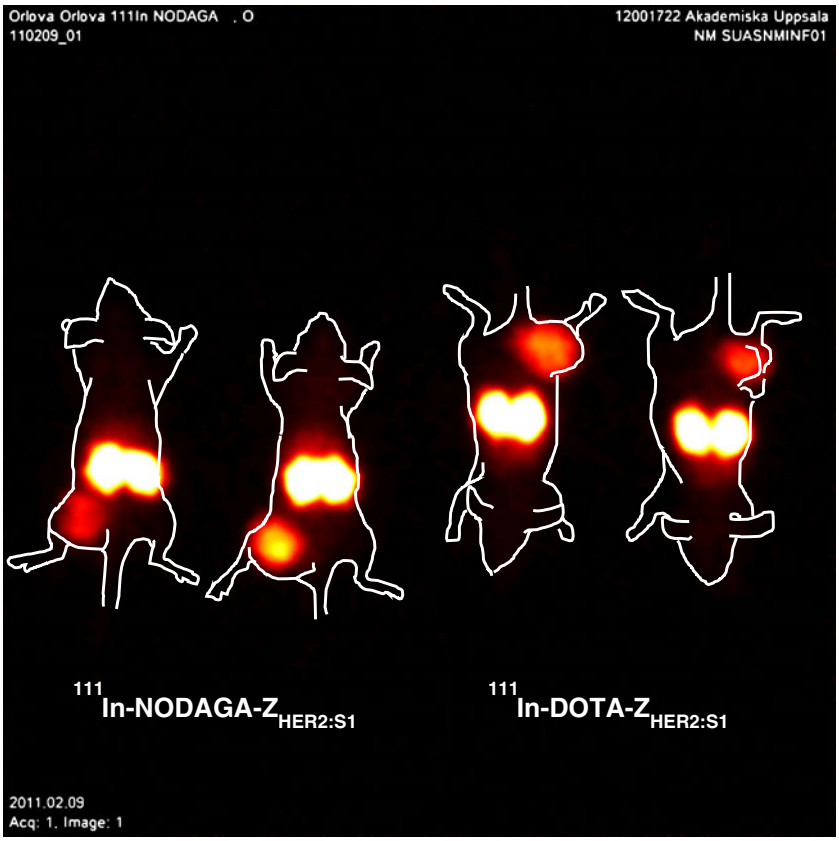

Fig. 5 Anterior gamma-camera images of nude mice bearing DU-145 xenografts 4 h after injection of ^{111}In-DOTA-$Z_{HER2:S1}$ and ^{111}In-NODAGA-$Z_{HER2:S1}$. Contours derived from a digital photograph were superimposed over gamma-camera images to facilitate interpretation

The HER2-binding Affibody molecules used in this study were synthetically produced and the chelators were coupled as the last step of peptide synthesis. Thus, there is no risk for coupling of the chelators to the binding site, which could interfere with the molecular recognition. Another advantage of the method is that a homogeneous end product is obtained, resulting in reproducible biodistribution properties.

All synthetically produced Affibody molecules maintained a high in vitro binding specificity after labelling, as shown by an in vitro saturation assay. Pre-saturation with cold Affibody reduced uptake in all cell lines and for all compounds (Fig. 2). Evaluation of cellular processing of ^{111}In-NOTA-$Z_{HER2:S1}$, ^{111}In-DOTA-$Z_{HER2:S1}$ and ^{111}In-NODAGA-$Z_{HER2:S1}$ showed that ^{111}In-DOTA-$Z_{HER2:S1}$ and ^{111}In-NODAGA-$Z_{HER2:S1}$ were somewhat more rapidly internalized, which is favourable in the case of residualizing radiometal labels.

Biodistribution studies in normal mice demonstrated rapid blood clearance and an overall low uptake in non-excretory organs for ^{111}In-NOTA-$Z_{HER2:S1}$, ^{111}In-DOTA-$Z_{HER2:S1}$ and ^{111}In-NODAGA-$Z_{HER2:S1}$. While the general biodistribution profile looked similar for all conjugates, a significantly higher liver uptake could be observed for ^{111}In-NOTA-$Z_{HER2:S1}$. This would lead to reduced contrast (and, for this reason, sensitivity) in detection of HER2-expressing metastases in liver. For this reason, ^{111}In-NOTA-$Z_{HER2:S1}$ was excluded from further evaluation. It has to be noted that the local distribution of electric charges in the conjugates is different. ^{111}In-NOTA-$Z_{HER2:S1}$ carries a positive charge at the N-terminus, while ^{111}In-DOTA-$Z_{HER2:S1}$ and ^{111}In-NODAGA-$Z_{HER2:S1}$ both have a neutral polar N-terminus (Fig. 1). Previous studies have demonstrated [21] a correlation between N-terminal positive charge and increased hepatic uptake for Affibody molecules. The finding of this study supports further connection between positive charge at the N-terminus and elevated hepatic uptake, which is essential for further development of Affibody-based imaging agents.

Another essential finding was the more rapid clearance from blood of ^{111}In-NODAGA-$Z_{HER2:S1}$ in comparison with other conjugates. An influence of labelling chemistry on clearance rate was earlier observed for Affibody molecules [21, 23, 37, 38] and for radiolabelled short peptides [39–42]. These findings might have implications for targeting: on the one hand, more rapid blood clearance of non-bound tracer may provide better contrast, and on the other hand, this might decrease tumour uptake of the radioactivity due to reduced tracer bioavailability. This necessitated direct in vivo comparison of ^{111}In-DOTA-$Z_{HER2:S1}$ and ^{111}In-NODAGA-$Z_{HER2:S1}$ in tumour-bearing mice. Both conjugates demonstrated highly specific uptake in HER2-expressing PC xenografts. The study showed (Table 3 and Fig. 4) that ^{111}In-NODAGA-$Z_{HER2:S1}$ provided a twofold higher tumour-to-blood ratio, but somewhat lower uptake in tumour and lower tumour-to-liver, tumour-to-spleen and tumour-to-bone ratios.

One has to take into account the frequency of metastatic sites for selection of an imaging agent for a disseminated cancer. Locoregional soft tissue metastases are characteristic for PC. Both ^{111}In-DOTA-$Z_{HER2:S1}$ and ^{111}In-NODAGA-$Z_{HER2:S1}$ would, most likely, be equally efficient in visualization of HER2 expression in such metastases, as tumour-to-tissue ratios for relevant organs (muscle, colon) have similar values. Typically, distant PC metastases are situated in the bone or the bone marrow. In this situation, the tumour-to-bone ratio is the most important and as this value is appreciably higher for ^{111}In-DOTA-$Z_{HER2:S1}$, this imaging agent would be superior for imaging of HER2 in PC for selection of patients for HER2-targeted therapy.

Conclusion

The results of this study suggest that optimization of the labelling chemistry has the potential to further increase the sensitivity of molecular imaging using Affibody molecules. Even subtle differences in the chelator structure might change the imaging contrast. This is especially important when up-regulation of a molecular target causes moderate expression levels, which is the case in up-regulation of HER2 in PC.

Acknowledgement This study was supported by grants from the Swedish Cancer Society (Cancerfonden), the Swedish Research Council (Vetenskapsrådet) and the VINNOVA SAMBIO program.

Conflicts of interest None.

References

1. Signoretti S, Montironi R, Manola J, Altimari A, Tam C, Bubley G, et al. Her-2-neu expression and progression toward androgen independence in human prostate cancer. J Natl Cancer Inst 2000;92:1918–25.
2. Yarden Y, Sliwkowski MX. Untangling the ErbB signalling network. Nat Rev Mol Cell Biol 2001;2:127–37.
3. Craft N, Shostak Y, Carey M, Sawyers CL. A mechanism for hormone-independent prostate cancer through modulation of androgen receptor signaling by the HER-2/neu tyrosine kinase. Nat Med 1999;5:280–5.
4. Culig Z, Hobisch A, Cronauer MV, Radmayr C, Trapman J, Hittmair A, Bartsch G, Klocker H. Androgen receptor activation in prostatic tumor cell lines by insulin-like growth factor-I, keratinocyte growth factor, and epidermal growth factor. Cancer Res 1994;54:5474–8.
5. Gioeli D, Ficarro SB, Kwiek JJ, Aaronson D, Hancock M, Catling AD, White FM, Christian RE, Settlage RE, Shabanowitz J, Hunt DF, Weber MJ. Androgen receptor phosphorylation. Regulation and identification of the phosphorylation sites. J Biol Chem 2002;277:29304–14.
6. Scher HI, Sawyers CL. Biology of progressive, castration-resistant prostate cancer: directed therapies targeting the androgen-receptor signaling axis. J Clin Oncol 2005;23:8253–61.

7. So A, Gleave M, Hurtado-Col A, Nelson C. Mechanisms of the development of androgen independence in prostate cancer. World J Urol 2005;23:1–9.
8. Minner S, Jessen B, Stiedenroth L, Burandt E, Köllermann J, Mirlacher M, Erbersdobler A, Eichelberg C, Fisch M, Brümmendorf TH, Bokemeyer C, Simon R, Steuber T, Graefen M, Huland H, Sauter G, Schlomm T. Low level HER2 overexpression is associated with rapid tumor cell proliferation and poor prognosis in prostate cancer. Clin Cancer Res 2010;16:1553–60.
9. Bacus SS, Altomare DA, Lyass L, Chin DM, Farrell MP, Gurova K, Gudkov A, Testa JR. AKT2 is frequently upregulated in HER-2/neu-positive breast cancers and may contribute to tumor aggressiveness by enhancing cell survival. Oncogene 2002;21:3532–40.
10. Tolmachev V. Imaging of HER-2 overexpression in tumors for guiding therapy. Curr Pharm Des 2008;14:2999–3019.
11. Malmberg J, Tolmachev V, Orlova A. Imaging agents for in vivo molecular profiling of disseminated prostate cancer: cellular processing of [111In]-labeled CHX-A″ DTPA-trastuzumab and anti-HER2 ABY-025 Affibody in prostate cancer cell lines. Exp Ther Med 2011;2:523–8.
12. Löfblom J, Feldwisch J, Tolmachev V, Carlsson J, Ståhl S, Frejd FY. Affibody molecules: engineered proteins for therapeutic, diagnostic and biotechnological applications. FEBS Lett 2010;584:2670–80.
13. Ahlgren S, Tolmachev V. Radionuclide molecular imaging using Affibody molecules. Curr Pharm Biotechnol 2010;11:581–9.
14. Nygren PÅ. Alternative binding proteins: affibody binding proteins developed from a small three-helix bundle scaffold. FEBS J 2008;275:2668–76.
15. Orlova A, Magnusson M, Eriksson T, Nilsson M, Larsson B, Höidén-Guthenberg I, Widström C, Carlsson J, Tolmachev V, Ståhl S, Nilsson FY. Tumor imaging using a picomolar affinity HER2 binding Affibody molecule. Cancer Res 2006;66:4339–48.
16. Baum RP, Prasad V, Müller D, Schuchardt C, Orlova A, Wennborg A, Tolmachev V, Feldwisch J. Molecular imaging of HER2-expressing malignant tumors in breast cancer patients using synthetic 111In- or 68Ga-labeled affibody molecules. J Nucl Med 2010;51:892–7.
17. Malmberg J, Sandström M, Wester K, Tolmachev V, Orlova A. Comparative biodistribution of imaging agents for in vivo molecular profiling of disseminated prostate cancer (PC) in mice bearing PC xenografts: focus on 111In- and 125I-labeled anti-HER2 humanized monoclonal trastuzumab and ABY-025 Affibody. Nucl Med Biol 2011. doi:10.1016/j.nucmedbio.
18. Engfeldt T, Orlova A, Tran T, Bruskin A, Widström C. Eriksson Karlström A, Tolmachev V. Imaging of HER2-expressing tumours using a synthetic Affibody molecule containing the 99mTc-chelating mercaptoacetyl-glycyl-glycyl-glycyl (MAG3) sequence. Eur J Nucl Med Mol Imaging 2007;34:722–33.
19. Engfeldt T, Tran T, Orlova A, Widström C, Eriksson Karlström A, Tolmachev V. 99mTc-chelator engineering to improve tumour targeting properties of a HER2-specific Affibody molecule. Eur J Nucl Med Mol Imaging 2007;34:1843–53.
20. Tran T, Engfeldt T, Orlova A, Sandström M, Feldwisch J, Abrahmsén L, Wennborg A, Tolmachev V, Eriksson Karlström A. (99m)Tc-maEEE-Z(HER2:342), an Affibody molecule-based tracer for detection of HER2 expression in malignant tumors. Bioconjug Chem 2007;18:1956–64.
21. Tran T, Ekblad T, Orlova A, Sandström M, Feldwisch J, Wennborg A, Abrahmsén L, Tolmachev V, Eriksson Karlström A. Effects of lysine-containing mercaptoacetyl-based chelators on the biodistribution of 99mTc-labeled anti-HER2 Affibody molecules. Bioconjug Chem 2008;19:2568–76.
22. Ekblad T, Tran T, Orlova A, Widström C, Feldwisch J, Abrahmsén L, Wennborg A, Eriksson Karlström A, Tolmachev V. Development and preclinical characterisation of 99mTc-labelled Affibody molecules with reduced renal uptake. Eur J Nucl Med Mol Imaging 2008;35:2245–55.
23. Wållberg H, Orlova A, Altai M, Hosseinimehr SJ, Widström C, Malmberg J, Ståhl S, Tolmachev V. Molecular design and optimization of 99mTc-labeled recombinant affibody molecules improves their biodistribution and imaging properties. J Nucl Med 2011;52:461–9.
24. Tolmachev V, Altai M, Sandström M, Perols A, Eriksson Karlström A, Boschetti F, Orlova A. Evaluation of a maleimido derivative of NOTA for site-specific labeling of Affibody molecules. Bioconjug Chem 2011;22:894–902.
25. De León-Rodríguez LM, Kovacs Z. The synthesis and chelation chemistry of DOTA-peptide conjugates. Bioconjug Chem 2008;19:391–402.
26. Eisenwiener KP, Prata MI, Buschmann I, Zhang HW, Santos AC, Wenger S, Reubi JC, Mäcke HR. NODAGATOC, a new chelator-coupled somatostatin analogue labeled with [67/68Ga] and [111In] for SPECT, PET, and targeted therapeutic applications of somatostatin receptor (hsst2) expressing tumors. Bioconjug Chem 2002;13:530–41.
27. Engfeldt T, Renberg B, Brumer H, Nygren PÅ, Eriksson Karlström A. Chemical synthesis of triple-labelled three-helix bundle binding proteins for specific fluorescent detection of unlabelled protein. Chembiochem 2005;6:1043–50.
28. Ross JS, Fletcher JA, Bloom KJ, Linette GP, Stec J, Symmans WF, Pusztai L, Hortobagyi GN. Targeted therapy in breast cancer: the HER-2/neu gene and protein. Mol Cell Proteomics 2004;3:379–98.
29. Persson M, Tolmachev V, Andersson K, Gedda L, Sandström M, Carlsson J. [(177)Lu]pertuzumab: experimental studies on targeting of HER-2 positive tumour cells. Eur J Nucl Med Mol Imaging 2005;32:1457–62.
30. Wållberg H, Orlova A. Slow internalization of anti-HER2 synthetic affibody monomer 111In-DOTA-ZHER2:342-pep2: implications for development of labeled tracers. Cancer Biother Radiopharm 2008;23:435–42.
31. Pienta KJ, Bradley D. Mechanisms underlying the development of androgen-independent prostate cancer. Clin Cancer Res 2006;12:1665–71.
32. Nielsen DL, Andersson M, Kamby C. HER2-targeted therapy in breast cancer. Monoclonal antibodies and tyrosine kinase inhibitors. Cancer Treat Rev 2009;35:121–36.
33. De Vita F, Giuliani F, Silvestris N, Catalano G, Ciardiello F, Orditura M. Human epidermal growth factor receptor 2 (HER2) in gastric cancer: a new therapeutic target. Cancer Treat Rev 2010;36 Suppl 3:S11–5.
34. Ziada A, Barqawi A, Glode LM, Varella-Garcia M, Crighton F, Majeski S, Rosenblum M, Kane M, Chen L, Crawford ED. The use of trastuzumab in the treatment of hormone refractory prostate cancer; phase II trial. Prostate 2004;60:332–7.
35. Lara Jr PN, Chee KG, Longmate J, Ruel C, Meyers FJ, Gray CR, Edwards RG, Gumerlock PH, Twardowski P, Doroshow JH, Gandara DR. Trastuzumab plus docetaxel in HER-2/neu-positive prostate carcinoma: final results from the California Cancer Consortium Screening and Phase II Trial. Cancer 2004;100:2125–31.
36. Sridhar SS, Hotte SJ, Chin JL, Hudes GR, Gregg R, Trachtenberg J, Wang L, Tran-Thanh D, Pham NA, Tsao MS, Hedley D, Dancey JE, Moore MJ. A multicenter phase II clinical trial of lapatinib (GW572016) in hormonally untreated advanced prostate cancer. Am J Clin Oncol 2010;33:609–13.
37. Tolmachev V, Velikyan I, Sandström M, Orlova A. A HER2-binding Affibody molecule labelled with 68Ga for PET imaging: direct in vivo comparison with the 111In-labelled analogue. Eur J Nucl Med Mol Imaging 2010;37:1356–67.
38. Tolmachev V, Hofström C, Malmberg J, Ahlgren S, Hosseinimehr SJ, Sandström M, Abrahmsén L, Orlova A, Gräslund T.

HEHEHE-tagged affibody molecule may be purified by IMAC, is conveniently labeled with [99(m)Tc(CO)3](+), and shows improved biodistribution with reduced hepatic radioactivity accumulation. Bioconjug Chem 2010;21:2013–22.
39. de Jong M, Bakker WH, Krenning EP, Breeman WA, van der Pluijm ME, Bernard BF, Visser TJ, Jermann E, Béhé M, Powell P, Mäcke HR. Yttrium-90 and indium-111 labelling, receptor binding and biodistribution of [DOTA0, d-Phe1, Tyr3]octreotide, a promising somatostatin analogue for radionuclide therapy. Eur J Nucl Med 1997;24:368–71.
40. Froidevaux S, Heppeler A, Eberle AN, Meier AM, Häusler M, Beglinger C, Béhé M, Powell P, Mäcke HR. Preclinical comparison in AR4-2J tumor-bearing mice of four radiolabeled 1,4,7,10-tetraazacyclododecane-1,4,7,10-tetraacetic acid-somatostatin analogs for tumor diagnosis and internal radiotherapy. Endocrinology 2000;141:3304–12.
41. Froidevaux S, Calame-Christe M, Schuhmacher J, Tanner H, Saffrich R, Henze M, Eberle AN. A gallium-labeled DOTA-alpha-melanocyte- stimulating hormone analog for PET imaging of melanoma metastases. J Nucl Med 2004;45:116–23.
42. Decristoforo C, Hernandez Gonzalez I, Carlsen J, Rupprich M, Huisman M, Virgolini I, Wester HJ, Haubner R. 68Ga- and 111In-labelled DOTA-RGD peptides for imaging of alphavbeta3 integrin expression. Eur J Nucl Med Mol Imaging 2008;35:1507–15.